Periodic and solitary waves in an inhomogeneous optical waveguide with third-order dispersion and self-steepening nonlinearity

Vladimir I. Kruglov[1] and Houria Triki[2]
[1]*Centre for Engineering Quantum Systems, School of Mathematics and Physics, The University of Queensland, Brisbane, Queensland 4072, Australia*
[2]*Radiation Physics Laboratory, Department of Physics, Faculty of Sciences, Badji Mokhtar University, P.O. Box 12, 23000 Annaba, Algeria*

(Received 14 October 2020; accepted 14 January 2021; published 28 January 2021)

We demonstrate the formation of periodic waves and envelope solitons in dispersive optical media having a Kerr nonlinear response under the influence of third-order dispersion and self-steepening effect. The stability properties of the bright- and dark-soliton solutions are proved using the stability criterion based on the theory of nonlinear dispersive waves. Regimes for the modulation instability of a continuous wave signal propagating inside the dispersive optical medium are also investigated. The results show that the gain spectrum depends crucially on the self-steepening parameter, while the third-order dispersion has no effect on the modulation instability condition. A similarity transformation is presented to reduce the generalized extended nonlinear Schrödinger equation with distributed coefficients which models the pulse evolution in the presence of the inhomogeneities of media to the related constant-coefficient one. The propagation behaviors of self-similar bright and dark solitons are discussed in a periodic distributed fiber system and an exponential dispersion decreasing fiber.

DOI: 10.1103/PhysRevA.103.013521

I. INTRODUCTION

Solitons are shape-preserving waves that have been observed experimentally in different physical media, such as monomode fibers [1], femtosecond lasers [2], and bulk optical materials [3]. The formation of these special wave packets occurs when the dispersion or diffraction associated with the finite size of the wave is exactly balanced by the nonlinear change of the properties of material induced by the wave itself. Of particular interest are soliton pulses that propagate in optical fibers because of their enormous potential for telecommunication and ultrafast signal-routing systems [4]. Their remarkable robustness makes them the most suitable means for processing bits of information [5]. There are two different soliton types, dark and bright solitons, which can propagate along an optical fiber without changing their shapes, and attenuation due to the intensity-dependent refractive index of the fiber exactly compensates for the pulse-spreading effects of group-velocity dispersion. A dark-soliton pulse can form in the normal dispersion regime, which appears in the form of a dip against a uniform background [6]. Unlike the dark soliton, a bright soliton is a pulse on a zero-intensity background which could arise in the anomalous dispersion regime of the fiber spectrum [7]. Usually, the soliton dynamics is governed by the cubic nonlinear Schrödinger equation (NLSE) that includes terms accounting for the group-velocity dispersion (GVD) and self-phase modulation [4]. This model is valid if the assumption that the spatial width of the soliton is much larger than the carrier wavelength is satisfied. This is equivalent to the condition that the width of the soliton frequency spectrum is much less than the carrier frequency [8]. It may be relevant to mention that the NLSE model is used to describe the propagation of both temporal and spatial envelope solitons in fibers and planar waveguides, respectively [9]. Recently, Song *et al.* [10] presented experimentally verified optical solitons in fiber lasers. Note that optical soliton formation in such dissipative nonlinear optical systems is a result of the mutual interaction among the fiber nonlinearity, cavity dispersion, laser gain saturation, and gain bandwidth filtering. Recent studies have shown that fiber lasers also provide an ideal platform to observe the generation of optical rogue waves and study their behavior [11]. Interestingly, vector solitons were also experimentally observed in black phosphorus mode-locked fiber lasers [12].

For increasing the bit rate further, it is desirable to use ultrashort (femtosecond) pulses. More precisely, high bit rates correspond to narrow pulse widths per channel [13]. It is worth mentioning that the application of such femtosecond pulses is restricted not only to ultrahigh-bit-rate optical communication systems but also to the ultrafast physical processes, optical sampling systems, and infrared time-resolved spectroscopy [4,14]. Thus, the importance of femtosecond light pulses is extensive. However, experimental and theoretical studies have shown that higher-order effects should be taken into account for femtosecond pulse propagation in a monomode optical fiber and the extended NLSE should be employed to describe its evolution [15,16]. The most general effects that become increasingly important as pulses get shorter are the third-order dispersion, self-steepening (i.e., Kerr dispersion), and the self-frequency shift. Because the spectral width of the ultrashort light pulses becomes comparable to the carrier frequency, these additional effects should

be considered [17]. All these effects will give some additional perturbation to the soliton system. Notably, the behavior of ultrashort pulses changes under the influence of these additional effects. For example, third-order dispersion produces a considerable amount of asymmetrical broadening in the time domain for ultrashort pulses [18] and results in radiation phenomena [19]. Also, self-steepening that arises when the group velocity of a pulse depends on the intensity [20] forces the peak of the pulse to travel slower than the wings and consequently causes an asymmetrical spectral broadening of the pulse [18]. Apart from third-order dispersion and self-steepening nonlinearity, the ultrashort pulse will also suffer from many other higher-order dispersive and nonlinear effects as it become extremely short (below 10 fs). Importantly, when the intensity of the light pulses crosses a certain threshold value the optical fiber behaves nonlinearly [21]. It should be noted that the magnitude of a given higher-order effect in single-mode fibers is dependent not only on the optical pulse but also on the fiber parameters.

Naturally, an appropriate modeling of the propagation characteristics of optical fibers should readily include the influence of various physical phenomena on short-pulse propagation and generation. To theoretically describe the evolution of femtosecond pulses through a nonlinear fiber, the nonlinear Schrödinger (NLS) family of equations incorporating additional corrections terms is widely used with constant or variable coefficients [22–25]. From a theoretical point of view, the inclusion of extra terms to model ultrashort pulses changes drastically integrability properties of the NLSE. Generally, the addition of further higher-order dispersive and nonlinear terms to the cubic NLS model produces an equation which is generally not integrable.

Recently, the influence of various higher-order effects on the propagation of light pulses has attracted a great deal of interest. This should not be surprising because these effects may add qualitatively certain novel properties to the wave propagation phenomena which are important in many practical applications (e.g., W-shaped and M-shaped solitons, modulational instability, rogue waves, and breathers) [24–29]. For example, Akhmediev and Karsson [26] investigated the amount of radiation emitted by solitons due to higher-order dispersion in optical fibers. Artigas *et al.* [27] studied the effect of quintic nonlinearities in the propagation of solitons in cubic nonlinear media. Moreover, Li *et al.* [28] demonstrated a novel W-shaped solitary-wave structure in an optical fiber with higher-order effects such as third-order dispersion, self-steepening, and the self-frequency shift effect. Recent studies also reported the existence of a dipole solitary wave in highly nonlinear optical fibers exhibiting quintic non-Kerr nonlinearities [29]. Furthermore, the present authors demonstrated in recent papers [30,31] that a generalized NLSE allows for the existence of quartic and dipole solitons in the presence of an additional self-steepening term and without a self-steepening term as well. The model incorporating the contribution of all orders of dispersion up to the fourth order as well as self-steepening nonlinearity applies to the description of femtosecond optical pulse propagation in silicon-based slot waveguides. The experimental observation of quartic and dipole solitons is possible, for example, in a silicon-on-insulator waveguide fabricated along a specific direction on the surface. However, less attention has been paid to the study of different types of solitons in optical fibers with third-order dispersion and self-steepening effects.

The intrapulse Raman scattering plays the most important role among the higher-order nonlinear effects [15,32]. The stimulated Raman scattering leads to a continuous downshift of the soliton carrier frequency when the pulse spectrum becomes so broad that the high-frequency components of a pulse can transfer energy to low-frequency components of the same pulse through Raman amplification. The Raman-induced frequency shift is negligible for the pulse width $\tau_0 > 10$ fs and it becomes of considerable importance for the short soliton width $\tau_0 < 5$ fs. However, it turns out that pulselike solitons do not exist when the Raman term is included because the resulting perturbation is non-Hamiltonian type. Physically, the Raman-induced spectral redshift does not preserve pulse energy because a part of the energy is dissipated through the excitation of molecular vibrations. However, a kink-type topological soliton (with infinite energy) has been found. The recent advent of photonics based on silicon-on-insulator (SOI) technology allows design slot waveguides for silicon and silica or silicon nanocrystals. The important possibility of such technology is that for a SOI waveguide fabricated along the special direction $[\bar{1}10]$ on the $[110] \times [001]$ surface, stimulated Raman scattering cannot occur when an input pulse excites the quasi-transverse-magnetic (quasi-TM) mode of the waveguide [33,34].

In this paper we analyze the existence, propagation properties, and stability of solitary light waves in an optical Kerr medium exhibiting these effects. The successive approach we develop here allows us to describe the propagation dynamics of two different types of solitons, bright and dark, in the presence of the third order of the fiber dispersion and self-steepening process. This approach also enables us to find the specific soliton characteristics in terms of all physical parameters. Our results include also investigations of the modulational instability and self-similar solitary-pulse propagation in the optical fiber system. It is shown that the self-similar solitary-wave shape and dynamical behavior can be controlled by selecting the third-order dispersion and gain or loss parameters appropriately.

The rest of the paper is organized as follows. Section II presents a regular method which yields the traveling-wave solutions of an extended NLSE with third-order dispersion and self-steepening terms, describing the propagation of femtosecond light pulses in dispersive optical fibers having a Kerr-type nonlinear response. Section III introduces exact periodic bounded and unbounded wave solutions as well as soliton solutions of the model. Section IV is devoted to stability analysis of the obtained soliton solutions based on the theory of optical nonlinear dispersive waves. We examine the modulational instability of a continuous wave signal propagating inside the fiber medium in Sec. V. By means of the similarity transformation method, we construct self-similar soliton solutions of the generalized nonlinear Schrödinger equation with distributed coefficients governing the pulse evolution in the presence of the inhomogeneities of fiber media in Sec. VI. We also investigate here the dynamical behaviors of those self-similar solitons in a specified soliton control system. In Sec. VII we present a physical discussion and

results showing the influence of higher-order effects on soliton dynamics. Finally, we present a summary and our main conclusions in Sec. VIII.

II. TRAVELING WAVES OF THE EXTENDED NONLINEAR SCHRÖDINGER EQUATION

For ultrashort light pulses whose duration is shorter than 100 fs, the optical field [i.e., $\psi(z,\tau)$] in a nonlinear optical fiber with third-order dispersion and self-steepening nonlinearity is modeled by the extended NLSE [15]

$$i\frac{\partial\psi}{\partial z}=\alpha\frac{\partial^2\psi}{\partial\tau^2}+i\sigma\frac{\partial^3\psi}{\partial\tau^3}-\gamma|\psi|^2\psi-i\nu\frac{\partial}{\partial\tau}(|\psi|^2\psi), \quad (1)$$

where z is the longitudinal coordinate, $\tau=t-\beta_1 z$ is the retarded time, $\alpha=\beta_2/2$, $\sigma=\beta_3/6$, and γ is the nonlinear parameter. The parameter $\beta_k=(d^k\beta/d\omega^k)_{\omega=\omega_0}$ is the kth-order dispersion of the optical fiber, $\beta(\omega)$ is the propagation constant depending on the optical frequency, and $\nu=\gamma/\omega_0$ is self-steepening coefficient.

The intrapulse Raman scattering effects are governed by the term $\gamma\tau_R\psi\partial(|\psi|^2)/\partial\tau$, which in general must be added to the right-hand side of the extended NLSE (1). Here τ_R is the Raman parameter with a value of about 3 fs for silica fiber. Note that pulselike solitons do not exist when the Raman term is included in the extended NLSE (1). However, as discussed in Sec. I, the Raman effect is absent for specially designed slot waveguides based on silicon and silica or silicon nanocrystals excited with quasi-TM polarized pulses along the special direction on the surface of waveguide. In this case an intrapulse Raman scattering disappears and the propagation of femtosecond optical solitons is governed by Eq. (1).

In the limit of vanishing third-order dispersion (i.e., $\sigma=0$), Eq. (1) reduces to the derivative NLSE [35,36], which describes the optical soliton propagation in the presence of Kerr dispersion. In Ref. [37] special conditions were considered to derive the exact N-soliton solutions of Eq. (1) by use of the Hirota direct method. Here instead we analyze the existence of periodic waves and solitons without taking into account such conditions. We will mainly demonstrate that the balance among GVD, Kerr nonlinearity, third-order dispersion, and self-steepening effects in the optical fiber system enables the formation of different types localized pulses with interesting properties. Remarkably, the results presented below show that the NLSE model (1) allows general periodic and soliton solutions, in the sense that no *a priori* restrictions on equation parameters are assumed.

To search for exact solitary-wave solutions of Eq. (1), we consider a solution of the form

$$\psi(z,\tau)=u(x)\exp[i(\kappa z-\delta\tau+\phi)], \quad (2)$$

where $u(x)$ is a real function depending on the variable $x=\tau-qz$, with $q=v^{-1}$ the inverse velocity. Here κ and δ are the corresponding real parameters describing the wave number and frequency shift, while ϕ represents the phase of the pulse at $z=0$.

Substituting Eq. (2) into Eq. (1) and removing the exponential term, we obtain the system of two ordinary differential equations

$$\sigma\frac{d^3u}{dx^3}+(q-2\alpha\delta-3\sigma\delta^2-3\nu u^2)\frac{du}{dx}=0, \quad (3)$$

$$(\alpha+3\sigma\delta)\frac{d^2u}{dx^2}+(\kappa-\alpha\delta^2-\sigma\delta^3)u-(\gamma+\nu\delta)u^3=0. \quad (4)$$

Integration of Eq. (3) yields

$$\sigma\frac{d^2u}{dx^2}+(q-2\alpha\delta-3\sigma\delta^2)u-\nu u^3=C, \quad (5)$$

where C is the integration constant. We choose below $C=0$ and then Eq. (4) is equivalent to Eq. (5) in the case when the following two relations are satisfied:

$$\frac{\kappa-\alpha\delta^2-\sigma\delta^3}{\alpha+3\sigma\delta}=\frac{1}{\sigma}(q-2\alpha\delta-3\sigma\delta^2), \quad (6)$$

$$\frac{\gamma+\nu\delta}{\alpha+3\sigma\delta}=\frac{\nu}{\sigma}. \quad (7)$$

Equations (6) and (7) lead to the frequency shift δ and wave number κ as

$$\delta=\frac{\gamma}{2\nu}-\frac{\alpha}{2\sigma}, \quad (8)$$

$$\kappa=\alpha\delta^2+\sigma\delta^3+\frac{1}{\sigma}(\alpha+3\sigma\delta)(q-q_0), \quad q_0=2\alpha\delta+3\sigma\delta^2. \quad (9)$$

Thus the system of equations (4) and (5) reduces to the nonlinear ordinary differential equation

$$\frac{d^2u}{dx^2}+au+bu^3=0, \quad (10)$$

with the parameters a and b given by

$$a=\frac{q-q_0}{\sigma}, \quad b=-\frac{\nu}{\sigma}, \quad (11)$$

where $q_0=2\alpha\delta+3\sigma\delta^2$. We emphasize that the parameter $q=v^{-1}$ in Eqs. (9) and (11) is an arbitrary quantity which is in some interval connected with the appropriate solution of the extended NLSE (1). Integration of Eq. (10) yields the first-order nonlinear differential equation

$$\left(\frac{du}{dx}\right)^2+au^2+\frac{1}{2}bu^4=C_0, \quad (12)$$

where C_0 is an integration constant. We define a function $Y(x)$ by the relation

$$u(x)=\pm\sqrt{\frac{Y(x)}{2b}}, \quad (13)$$

which transforms Eq. (12) to the form

$$\left(\frac{dY}{dx}\right)^2=-(Y-Y_1)(Y-Y_2)(Y-Y_3). \quad (14)$$

In Eq. (14) the quantities Y_1, Y_2, and Y_3 are the roots of the cubic equation

$$Y^3+4aY^2-8C_0bY=0. \quad (15)$$

We consider in the following section different cases which yield the periodic bounded and unbounded solutions and solitary waves.

III. PERIODIC BRIGHT-SOLITON AND DARK-SOLITON SOLUTIONS

In this section we derive the periodic bounded and unbounded solutions of the extended NLSE (1). The limiting cases of these periodic-wave solutions lead to the bright-soliton and dark-soliton solutions. The general solution of Eq. (14) is given by

$$\pm\int \frac{dY}{\sqrt{(Y_1-Y)(Y_2-Y)(Y_3-Y)}} = x-\eta, \tag{16}$$

where η is an integration constant. We consider three cases: (i) $a<0$ and $b>0$, (ii) $a>0$ and $b<0$, and (iii) $a=0$ and $b>0$.

First we consider the case with $a<0$. The bounded solutions exist when the roots in Eq. (15) are real. We consider the case when these roots are real and different. We can order these roots as $Y_1<Y_2<Y_3$ and then we have the ordered roots $Y_1=0$, $Y_2=-2a(1-\lambda)$, and $Y_3=-2a(1+\lambda)$, where $\lambda=\sqrt{1+2C_0b/a^2}$. The parameter λ is an arbitrary quantity because C_0 is the integration constant. Note that the parameter λ is in an interval $0<\lambda<1$ because we assume that all these roots are real, different, and ordered. The periodic bounded solution given by Eq. (16) exists when the function $Y(x)$ is defined in the interval $Y_2\leqslant Y(x)\leqslant Y_3$. The explicit form of this periodic bounded solution is

$$Y(x)=Y_2+(Y_3-Y_2)\mathrm{cn}^2(w(x-\eta),k), \tag{17}$$

where $\mathrm{cn}(z,k)$ is the elliptic Jacobi function. The parameters w and k in this solution are

$$w=\frac{1}{2}\sqrt{Y_3-Y_1}=\sqrt{-\frac{a}{2}(1+\lambda)}, \tag{18}$$

$$k=\sqrt{\frac{Y_3-Y_2}{Y_3-Y_1}}=\sqrt{\frac{2\lambda}{1+\lambda}}. \tag{19}$$

Note that Eq. (17) yields an inequality $Y(x)>0$, and hence one should choose $b>0$ because we have the relation $u(x)=\pm\sqrt{Y(x)/2b}$. Thus we find the bounded periodic solution

$$u(x)=\pm\sqrt{-\frac{a}{b}}\{1-\lambda+2\lambda\,\mathrm{cn}^2(w(x-\eta),k)\}^{1/2}. \tag{20}$$

Note that the parameter k in this solution is defined in the interval $0<k<1$ because the parameter λ is in the interval $0<\lambda<1$. However, the solutions with $\lambda=0$ and 1 ($k=0$ and 1) follow from Eq. (20) as limiting cases. We present below the solutions of Eq. (1) based on the solution in Eq. (20).

A. Periodic bounded waves with $a<0$ and $b>0$

Equations (2) and (20) lead to a family of periodic bounded solutions with $0<\lambda<1$ as

$$\psi(z,\tau)=\Lambda[1-\lambda+2\lambda\,\mathrm{cn}^2(w\xi,k)]^{1/2}\exp[i(\kappa z-\delta\tau+\phi)], \tag{21}$$

where $\xi=\tau-qz-\eta$, with η the position of pulse at $z=0$, and $k=\sqrt{2\lambda/(1+\lambda)}$, with $0<\lambda<1$. The frequency shift δ and wave number κ are given in Eqs. (8) and (9). The amplitude Λ and parameter w in this solution are

$$\Lambda=\pm\sqrt{\frac{(q-q_0)}{\nu}},\quad w=\sqrt{-\frac{(q-q_0)(1+\lambda)}{2\sigma}}, \tag{22}$$

where q is an arbitrary parameter. Hence this periodic solution exists when the following inequalities are satisfied: $(q-q_0)/\nu>0$ and $(q-q_0)/\sigma<0$. It follows from these relations that $\nu\sigma<0$.

B. Bright-soliton solution with $a<0$ and $b>0$

In the limiting case with $\lambda=1$ we have $k=1$. Thus the soliton solution follows from Eq. (22) as

$$\psi(z,\tau)=A\,\mathrm{sech}[w_0(\tau-qz-\eta)]\exp[i(\kappa z-\delta\tau+\phi)]. \tag{23}$$

The amplitude A and the inverse width w_0 of the soliton solution are

$$A=\pm\sqrt{\frac{2(q-q_0)}{\nu}},\quad w_0=\sqrt{-\frac{q-q_0}{\sigma}}, \tag{24}$$

where q is an arbitrary parameter. This soliton exists when the following inequalities are satisfied: $(q-q_0)/\nu>0$ and $(q-q_0)/\sigma<0$. It follows from these relations that the condition $\nu\sigma<0$ for this soliton solution is satisfied as well. This soliton solution has the energy and momentum integrals

$$E=\int_{-\infty}^{+\infty}|\psi(z,\tau)|^2d\tau=4\sqrt{-\frac{\sigma(q-q_0)}{\nu^2}}, \tag{25}$$

$$M=\frac{i}{2}\int_{-\infty}^{+\infty}\left(\psi\frac{\partial\psi^*}{\partial\tau}-\psi^*\frac{\partial\psi}{\partial\tau}\right)d\tau=\frac{2(\alpha\nu-\gamma\sigma)}{\nu\sigma}\sqrt{-\frac{\sigma(q-q_0)}{\nu^2}}. \tag{26}$$

Note that in the limiting case with $\lambda=0$ the solution in Eq. (21) is given by $\psi(z,\tau)=\Lambda\exp[i(\kappa z-\delta\tau+\phi)]$.

Now we consider the second case with $a>0$. The bounded solutions exist when the roots in Eq. (15) are real. We consider here the case when these roots are real and different. If the roots are ordered as $Y_1<Y_2<Y_3$, then we have the ordered roots $Y_1=-2a(1+\lambda)$, $Y_2=-2a(1-\lambda)$, and $Y_3=0$, with $\lambda=\sqrt{1+2C_0b/a^2}$. The parameter λ is in an interval $0<\lambda<1$ because we assume that all these roots are real, different, and ordered. The periodic bounded solution given by Eq. (16) exists when the function $Y(x)$ is defined in the interval $Y_2\leqslant Y(x)\leqslant Y_3$. Note that in this case $Y(x)\leqslant 0$ and hence we choose $b<0$ because $u(x)=\pm\sqrt{Y(x)/2b}$. Thus the periodic bounded solution given in Eqs. (13) and (16) is given by

$$u(x)=\Lambda\,\mathrm{sn}(w(x-\eta),k), \tag{27}$$

where $\mathrm{sn}(z,k)$ is the elliptic Jacobi function. The parameters Λ, w, and k of this solution are

$$\Lambda=\pm\sqrt{-\frac{a}{b}(1-\lambda)},\quad w=\sqrt{\frac{a}{2}(1+\lambda)},\quad k=\sqrt{\frac{1-\lambda}{1+\lambda}}. \tag{28}$$

The parameter k in Eq. (28) is defined in the interval $0<k<1$ because the parameter λ is in the interval $0<\lambda<1$. We

present below two solutions of Eq. (1) based on the solution given in Eq. (27).

C. Periodic bounded waves with $a > 0$ and $b < 0$

Equations (2) and (27) lead to a family of periodic bounded solutions with $0 < \lambda < 1$ as

$$\psi(z,\tau) = \Lambda\,\mathrm{sn}(w\xi, k)\exp[i(\kappa z - \delta\tau + \phi)], \tag{29}$$

where $\xi = \tau - qz - \eta$, with η the position of pulse at $z = 0$, and $k = \sqrt{(1-\lambda)/(1+\lambda)}$, with $0 < \lambda < 1$. The frequency shift δ and wave number κ are given in Eqs. (8) and (9). The amplitude Λ and parameter w in this solution are

$$\Lambda = \pm\sqrt{\frac{(q-q_0)(1-\lambda)}{\nu}}, \quad w = \sqrt{\frac{(q-q_0)(1+\lambda)}{2\sigma}}, \tag{30}$$

where q is an arbitrary parameter. Hence this periodic solution exists when the following inequalities are satisfied: $(q-q_0)/\nu > 0$ and $(q-q_0)/\sigma > 0$. It follows from these relations that $\nu\sigma > 0$.

D. Dark-soliton solution with $a > 0$ and $b < 0$

In the limiting case with $\lambda = 0$ we have $k = 1$. Thus the dark-soliton solution follows from Eq. (29) as

$$\psi(z,\tau) = B\tanh[w_0(\tau - qz - \eta)]\exp[i(\kappa z - \delta\tau + \phi)]. \tag{31}$$

The amplitude B and the inverse width w_0 of the dark-soliton solution are

$$B = \pm\sqrt{\frac{q-q_0}{\nu}}, \quad w_0 = \sqrt{\frac{q-q_0}{2\sigma}}, \tag{32}$$

where q is an arbitrary parameter. This dark-soliton solution exists when the following inequalities are satisfied: $(q-q_0)/\nu > 0$ and $(q-q_0)/\sigma > 0$. It follows from these relations that the condition $\nu\sigma > 0$ for this dark-soliton solution is satisfied as well. Note that the solution in Eq. (31) has a kink-type shape; however, the intensity $I(z,\tau) = |\psi(z,\tau)|^2$ of this nonlinear wave has the dark-soliton profile.

Now we consider the third case with $a = 0$. The bounded solutions exist when the roots in Eq. (15) are real. We consider here the case when these roots are real and different. If the roots are ordered as $Y_1 < Y_2 < Y_3$, then we have the ordered roots $Y_1 = -\sqrt{8C_0 b}$, $Y_2 = 0$, and $Y_3 = \sqrt{8C_0 b}$, where C_0 is an integration constant. The periodic bounded solution given by Eq. (16) exists when the function $Y(x)$ is defined in the interval $Y_2 \leqslant Y(x) \leqslant Y_3$. Note that in this case $Y(x) \geqslant 0$ and hence we choose $b > 0$ because $u(x) = \pm\sqrt{Y(x)/2b}$. Thus the periodic bounded solution given in Eqs. (13) and (16) is

$$u(x) = \pm\sqrt{\frac{\mu}{b}}\,\mathrm{cn}(\sqrt{\mu}(x-\eta), k_0), \tag{33}$$

where $\mu = \sqrt{2C_0 b}$ and $k_0 = 1/\sqrt{2}$. In this solution we have $a = 0$, and hence the parameter $q = v^{-1}$ is fixed as $q = q_0$ with $q_0 = 2\alpha\delta + 3\sigma\delta^2$. Thus the variable x in this periodic solution is given by $x = \tau - q_0 z$. We present below the solution of Eq. (1) based on the solution given in Eq. (33).

E. Periodic bounded waves with $a = 0$ and $b > 0$

Equations (2) and (33) lead to a family of periodic bounded solutions with $\mu > 0$ as

$$\psi(z,\tau) = \Lambda\,\mathrm{cn}(w\xi, k_0)\exp[i(\kappa z - \delta\tau + \phi)], \tag{34}$$

where $\xi = \tau - q_0 z - \eta$, with q_0 given in Eq. (9). The parameter k_0 defining the elliptic Jacobi function in Eq. (34) is fixed as $k_0 = 1/\sqrt{2}$. The frequency shift δ is given in Eq. (8) and the wave number is $\kappa = \alpha\delta^2 + \sigma\delta^3$ because in this solution we have $q = q_0$. The amplitude Λ and parameter w in Eq. (34) are given by

$$\Lambda = \pm\sqrt{-\frac{\sigma\mu}{\nu}}, \quad w = \sqrt{\mu}, \tag{35}$$

where μ is an arbitrary parameter ($\mu > 0$). Hence this periodic solution exists when the inequality $\nu\sigma < 0$ is satisfied.

We also present the periodic unbounded solution of Eq. (10) given by

$$u(x) = \Lambda\frac{\mathrm{sn}(w(x-\eta), k)}{1 + \mathrm{cn}(w(x-\eta), k)}, \tag{36}$$

where the parameters Λ and w are

$$\Lambda = \pm\sqrt{-\frac{a}{b(2k^2-1)}}, \quad w = \sqrt{\frac{2a}{2k^2-1}}. \tag{37}$$

In this solution an arbitrary parameter k is in the interval $0 \leqslant k < 1/\sqrt{2}$ or the interval $1/\sqrt{2} < k < 1$.

F. Family of periodic unbounded waves

Equations (2) and (36) lead to a family of periodic unbounded solutions as

$$\psi(z,\tau) = \Lambda\,\frac{\mathrm{sn}(w\xi, k)}{1 + \mathrm{cn}(w\xi, k)}\exp[i(\kappa z - \delta\tau + \phi)], \tag{38}$$

where $\xi = \tau - qz - \eta$ and an arbitrary parameter k is in the interval $0 \leqslant k < 1/\sqrt{2}$ or the interval $1/\sqrt{2} < k < 1$. The frequency shift δ and wave number κ are given in Eqs. (8) and (9). The amplitude Λ and parameter w in this solution are

$$\Lambda = \pm\sqrt{\frac{(q-q_0)}{\nu(2k^2-1)}}, \quad w = \sqrt{\frac{2(q-q_0)}{\sigma(2k^2-1)}}. \tag{39}$$

These unbounded waves exist under the conditions $(q-q_0)/\nu(2k^2-1) > 0$ and $(q-q_0)/\sigma(2k^2-1) > 0$. In the limiting case with $k = 0$ the solution in Eq. (38) yields the periodic unbounded waves

$$\psi(z,\tau) = \pm\sqrt{-\frac{q-q_0}{\nu}}\tan(w_0\xi)\exp[i(\kappa z - \delta\tau + \phi)], \tag{40}$$

with $w_0 = \sqrt{-(q-q_0)/2\sigma}$. We note that in the limiting case with $k \to 1$ the unbounded solution in Eq. (38) transforms to dark-soliton solution given by Eq. (31).

In the Conclusion we emphasize that the solutions presented in this section significantly differ from solutions of the ordinary NLSE with $\sigma = 0$ and $\nu = 0$. This is apparent because the solutions presented have no sense in the limit when $\sigma \to 0$ and $\nu \to 0$. We emphasize that the solutions of the extended NLSE (1) obtained in this section have relevance

for the experiments on the short-pulse propagation in optical fiber communications, ultrafast lasers, and slow-light devices. Together with the fact that the Raman effect is absent for specially designed slot waveguides (see the discussion presented in Secs. I and II), the above periodic and solitary solutions can find various practical applications. We also discuss the experimental observation of femtosecond optical solitons in the Conclusion. Note that experimental implementation of optical solitons is connected with the stability condition which is obtained in the following section based on the theory of nonlinear dispersive waves.

IV. STABILITY ANALYSIS OF SOLITARY WAVES

We consider in this section the analytical stability analysis of soliton solutions for the extended NLSE (1) based on the theory of nonlinear dispersive waves in nonlinear optics and fluid dynamics [30,31,38]. For our purposes, we develop the dynamics of dispersive waves in the form

$$\psi(z,\tau) = F(\omega)\exp[i\Theta(z,\tau)], \tag{41}$$

where the amplitude $F(\omega)$ and phase $\Theta(z,\tau)$ are real functions. The wave number k and frequency ω of nonlinear dispersive waves are given by

$$k(\omega) = \frac{\partial\Theta}{\partial z}, \quad \omega = -\frac{\partial\Theta}{\partial\tau}. \tag{42}$$

We have by definition that $\Theta_{z\tau} = k_\tau$ and $\Theta_{\tau z} = -\omega_z$, which yield

$$\frac{\partial\omega}{\partial z} + \frac{\partial k(\omega)}{\partial\tau} = 0. \tag{43}$$

We assume that $\omega(z,\tau) = \tilde{\omega}(Z,T)$ and $k(z,\tau) = \tilde{k}(Z,T)$, where $Z = \varepsilon z$ and $T = \varepsilon\tau$ with $\varepsilon \ll 1$, are slow variables. Here $\tilde{\omega}(Z,T)$ and $\tilde{k}(Z,T)$ are slowly varying functions of the variables Z and T. The substitution of Eq. (41) into the extended NLSE (1) leads to a series of nonlinear equations. The equation in the zeroth order to the small parameter ε is

$$k(\omega) = k_0(\omega) + \Gamma(\omega)F^2(\omega), \tag{44}$$

where $k_0(\omega)$ and $\Gamma(\omega)$ are

$$k_0(\omega) = \alpha\omega^2 + \sigma\omega^3, \quad \Gamma(\omega) = \gamma + \nu\omega. \tag{45}$$

The parameter $\Gamma(\omega) = \gamma(1+\omega/\omega_0)$ is the renormalized nonlinear coefficient γ by the self-steepening effect. Equations (1) and (41) in the first order to the small parameter ε yield

$$\frac{\partial F}{\partial z} + k'(\omega)\frac{\partial F}{\partial\tau} = -\frac{1}{2}k_0''(\omega)F\frac{\partial\omega}{\partial\tau} + 2\Gamma(\omega)FF'\frac{\partial F}{\partial\tau} - 2\nu F^2\frac{\partial F}{\partial\tau}, \tag{46}$$

with $k'(\omega) = dk(\omega)/d\omega$ and $F' = dF(\omega)/d\omega$. Thus Eq. (44) is the nonlinear dispersion relation and Eq. (46) is the equation for the amplitude $F(\omega)$ of nonlinear waves. Note that Eq. (43) for varying frequency $\omega(z,\tau)$ can also be written in the form

$$\frac{\partial\omega}{\partial z} + k'(\omega)\frac{\partial\omega}{\partial\tau} = 0, \tag{47}$$

where the function $k'(\omega)$ is

$$k'(\omega) = k_0''(\omega) + 2\Gamma(\omega)F(\omega)F'(\omega) + \nu F^2(\omega). \tag{48}$$

The nature of Eqs. (44)–(47) based on the method of slow variables can be hyperbolic or elliptic. We first consider the case when this system of equations is hyperbolic. The characteristics connected to the hyperbolic system of equations (46) and (47) are given by

$$\frac{d\tau}{dz} = k'(\omega), \quad \frac{d\omega}{dz} = 0, \tag{49}$$

$$\frac{dF}{dz} = F\frac{\partial\omega}{\partial\tau}\left(2\Gamma(\omega)(F')^2 - 2\nu FF' - \frac{1}{2}k_0''(\omega)\right). \tag{50}$$

It follows from Eq. (49) that $dF/dz = F'(\omega)d\omega/dz = 0$. Thus Eq. (50) yields

$$\frac{dF(\omega)}{d\omega} = \frac{\nu F(\omega)}{2\Gamma(\omega)} \pm \frac{1}{2}\sqrt{\frac{\nu^2F^2(\omega)}{\Gamma^2(\omega)} + \frac{k_0''(\omega)}{\Gamma(\omega)}}, \tag{51}$$

where $k_0''(\omega) = 2\alpha + 6\sigma\omega$. Equations (49)–(51) yield the characteristic equation

$$\frac{d\tau}{dz} = k_0'(\omega) + 2\nu F^2(\omega) \pm \Gamma(\omega)F(\omega)\sqrt{\frac{\nu^2F^2(\omega)}{\Gamma^2(\omega)} + \frac{k_0''(\omega)}{\Gamma(\omega)}}. \tag{52}$$

It follows from this equation that the system of equations (46) and (47) with infinitesimal amplitude $F(\omega)$ is hyperbolic when the condition $k_0''(\omega)/\Gamma(\omega) \geqslant 0$ is satisfied and the system of equations (46) and (47) with infinitesimal amplitude $F(\omega)$ is elliptic for the condition $k_0''(\omega)/\Gamma(\omega) < 0$.

Equations (51) and (52) lead to a physical interpretation of stability for the soliton solutions of the extended NLSE (1). We may suppose [31] that the soliton is stable when it cannot radiate the nonlinear dispersive waves. We note that the outgoing nonlinear dispersive waves with infinitesimal amplitude $F(\omega)$, connected to such a radiation process, exist only in the case when the above system of equations is hyperbolic. Moreover, in the case of elliptic equations the problem of optical pulse radiation is not correct from a mathematical point of view. For the infinitesimal amplitude $F(\omega)$ this takes place in the case when $k_0''(\omega)/\Gamma(\omega) < 0$. This relation follows from Eqs. (51) and (52) because the outgoing nonlinear dispersive waves do not exist when the square root in these equations is imaginary and hence the system of equations (51) and (52) is elliptic. Note that the inequality $k_0''(\omega)/\Gamma(\omega) < 0$ is satisfied in some domain $\mathcal{D}$ of parameters α, σ, γ, and ν. Thus this physical interpretation of the stability of the soliton solution yields the stability domain $\mathcal{D}_{st}$ for a given type of soliton.

Now we consider the stability condition for the soliton solutions given in Eq. (23) with the frequency $\delta = (\gamma\sigma - \alpha\nu)/2\nu\sigma$. Equation (52) at $\omega = \delta$ has the form

$$\frac{d\tau}{dz} = q_0 + 2\nu F^2(\delta) \pm \Gamma F(\delta)\sqrt{\frac{F^2(\delta)}{(\omega_0+\delta)^2} + \frac{k_0''(\delta)}{\gamma(1+\delta/\omega_0)}}, \tag{53}$$

with $\Gamma = \Gamma(\delta) = \gamma(1+\delta/\omega_0)$ and $k_0''(\delta) = 3\gamma\sigma/\nu - \alpha$. Note that the solutions of the extended NLSE (1) should satisfy the condition $|\delta|/\omega_0 \ll 1$, where ω_0 is the carrier frequency. Derivation of the extended NLSE (1) is based on this condition for the envelope of nonlinear waves. Hence Eq. (53) with infinitesimal amplitude $F(\delta)$ yields the criterion $k_0''(\delta)/\gamma < 0$ of the soliton stability. Thus the criterion of the

soliton stability for the solution in Eq. (23) is given by the inequality

$$\frac{\alpha}{\gamma} > \frac{3\sigma}{\nu}. \tag{54}$$

Using the relation $\nu = \gamma/\omega_0$, the criterion (54) can also be written as $\alpha\nu > 3\sigma\gamma$. Hence the criterion (54) can be written in the form

$$\nu\beta_2 > \gamma\beta_3. \tag{55}$$

Thus the necessary and sufficient conditions for stability of the bright soliton in Eq. (23) are given by the inequalities $(q - q_0)/\nu > 0$, $(q - q_0)/\sigma < 0$, and $\alpha\nu > 3\sigma\gamma$. We emphasize that the stability criterion formulated for the extended NLSE (1) can be applied to more general nonlinear Schrödinger equations which have the Hamiltonian form. We also note that the similarity transformation of the generalized NLSE developed in Sec. VI does not influence the stability of solitons because this similarity transformation is connected with scaling functions only.

V. MODULATIONAL INSTABILITY

An important phenomenon closely associated with the soliton formation is the occurrence of modulational instability (MI). It refers to a process in which the amplitude and phase modulations of a wave grow as a result of an interplay between the nonlinearity and dispersion [39]. In what follows, we examine the MI of a continuous wave (cw) propagating in a fiber system governed by the extended NLSE (1). This can be done by employing the standard linear stability analysis [4]. To study the process in detail, the cw solution will be perturbed first and then this small perturbation will be analyzed whether it grows or decays with propagation.

The steady-state solution of Eq. (1), corresponding to a cw signal, is given by

$$\psi(z, \tau) = \sqrt{P_0}\exp(i\phi_{\rm nl}), \tag{56}$$

where the nonlinear phase shift $\phi_{\rm nl}$ is related to the optical power P_0 and the propagation distance as $\phi_{\rm nl} = \gamma P_0 z$. The latter relation, together with Eq. (56), shows that the cw signal acquires only a power-dependent phase shift after propagation through the optical fiber. To examine the stability of such a steady-state solution, we add a small perturbation $a(z, \tau)$ to the cw light so that we have

$$\psi(z, \tau) = [\sqrt{P_0} + a(z, \tau)]\exp(i\phi_{\rm nl}), \tag{57}$$

where a small perturbation $a(z, \tau)$ satisfies the condition $|a(z, \tau)| \ll \sqrt{P_0}$. Hence, if the perturbed field grows exponentially, the steady state becomes unstable. Substituting Eq. (57) into Eq. (1), we get the linearized equation of the perturbed field as

$$ia_z = \alpha a_{\tau\tau} + i\sigma a_{\tau\tau\tau} - \gamma P_0(a + a^*) - i\nu P_0(2a_\tau + a_\tau^*), \tag{58}$$

where the asterisk denotes the complex conjugate. Now we make the ansatz for the perturbed field

$$a(z, \tau) = a_1\exp[i(Qz - \Omega\tau)] + a_2\exp[-i(Qz - \Omega\tau)], \tag{59}$$

where Q and Ω are, respectively, the wave number and the frequency of the modulation, while a_1 and a_2 are real amplitudes of infinitesimal perturbation.

With further substitution of this ansatz into Eq. (58), we can obtain a system of two homogeneous equations for a_1 and a_2. This system has a nontrivial solution only when Q and Ω satisfy the dispersion relation

$$Q = \sigma\Omega^3 + 2\nu P_0\Omega \pm |\Omega|\sqrt{f(\Omega)}, \tag{60}$$

where the function $f(\Omega)$ is given by

$$f(\Omega) = 2\alpha\gamma P_0 + \alpha^2\Omega^2 + \nu^2 P_0^2. \tag{61}$$

The steady state becomes unstable if the wave number Q has an imaginary part for some values of Ω since the small perturbation a experiences an exponential growth along the optical fiber length. This phenomenon is referred to as MI since it leads to the modulation of the steady-state amplitude [40]. The MI is measured by the power gain defined at any pump frequency Ω as $G(\Omega) = 2|{\rm Im}Q|$, where ${\rm Im}Q$ represents the imaginary part of Q. If we let $f(\Omega) < 0$ for the interval of frequencies $\Omega \in S$, $[\Omega^2 < -2\gamma P_0/\alpha - \nu^2 P_0^2/\alpha^2]$, then the corresponding gain spectrum is given by

$$G(\Omega) = 2|\Omega|\sqrt{-2\alpha\gamma P_0 - \alpha^2\Omega^2 - \nu^2 P_0^2} \tag{62}$$

for $\Omega \in S$ and $G(\Omega) = 0$ for $\Omega \notin S$.

We observe that only the GVD, Kerr nonlinearity, and self-steepening effects contribute to the MI gain spectrum. However, the third-order dispersion does not play any role in the gain spectrum. Also, the MI gain $G(\Omega)$ does not depend on the sign of the self-steepening parameter ν.

It follows from Eq. (60) that the plain wave will be modulation stable for the frequencies $f(\Omega) \geqslant 0$. This condition can be written in the form

$$\Omega^2 \geqslant -\frac{2\gamma P_0}{\alpha} - \frac{\nu^2 P_0^2}{\alpha^2}. \tag{63}$$

Thus, we see from the cases above that the modulation instability phenomenon studied within the extended NLSE (1) framework can exist not only in an anomalous GVD regime, but also in the normal GVD regime that uniquely depends on the values of Kerr nonlinearity and self-steepening parameters.

VI. SIMILARITY TRANSFORMATION OF THE GENERALIZED NLSE

Propagation of light pulses in optical fibers is understood completely if the inhomogeneities of media resulting from various factors such as the variation in lattice parameters of the fiber media and fluctuation of the fiber diameters are considered [41]. The inclusion of the variable coefficients in the governing NLSEs is currently an effective way to reflect the inhomogeneous effects of the nonlinear optical pulses [42]. In what follows, we discuss the wave propagation phenomenon in a realistic fiber system exhibiting varying third-order dispersion and self-steepening nonlinearity. An appropriate model equation for describing femtosecond pulse propagation through such an inhomogeneous optical fiber can be readily obtained by considering the variation with respect

to the propagation distance of all waveguide parameters in Eq. (1) resulting in the generalized NLSE with distributed coefficients

$$i\frac{\partial\Phi}{\partial s} = D_2(s)\frac{\partial^2\Phi}{\partial t^2} + iD_3(s)\frac{\partial^3\Phi}{\partial t^3} - R_1(s)|\Phi|^2\Phi - iR_2(s)\frac{\partial}{\partial t}(|\Phi|^2\Phi) + iG(s)\Phi, \tag{64}$$

where $D_2(s)$ and $D_3(s)$ are the variable parameters of GVD and third-order dispersions, respectively. The parameters $R_1(s)$ and $R_2(s)$ are related to the Kerr nonlinearity and self-steepening effect, respectively. Also $G(s)$ represents the amplification or absorption coefficient.

To connect solutions of Eq. (64) with those of Eq. (1), we will use the transformation [43–45] as

$$\Phi(s,t) = \rho(s)\psi(z(s),\tau(s,t))\exp[i\varphi(s,t)], \tag{65}$$

where the real quantities $\rho(s)$ and $\varphi(s,t)$ represent the amplitude and phase of the self-similar pulse, respectively. Also, $z(s)$ is an effective propagation distance to be determined, while $\tau(s,t)$ is the similarity variable depending on both s and t.

Substituting Eq. (65) into Eq. (64) leads to Eq. (1), but we must have the set of equations

$$\rho_s - G\rho - D_2A\varphi_{tt} + 3D_3A\varphi_t\varphi_{tt} = 0, \tag{66}$$

$$\tau_s - 2D_2\tau_t\varphi_t + 3D_3\tau_t\varphi_t^2 - D_3\tau_{ttt} = 0, \tag{67}$$

$$\varphi_s - D_2\varphi_t^2 - D_3\varphi_{ttt} + D_3\varphi_t^3 = 0, \tag{68}$$

$$(3D_3\varphi_t - D_2)\tau_{tt} + 3D_3\tau_t\varphi_{tt} = 0, \tag{69}$$

$$(R_1 - R_2\varphi_t)\rho^2 = \gamma z_s, \tag{70}$$

$$(D_2 - 3D_3\varphi_t)\tau_t^2 = \alpha z_s, \tag{71}$$

$$D_3\tau_t^3 = \sigma z_s, \tag{72}$$

$$\tau_{tt} = 0, \tag{73}$$

$$R_2\tau_t\rho^2 = \nu z_s. \tag{74}$$

Solving this set of equations self-consistently, we obtain the self-similar pulse parameters

$$z(s) = \frac{K^3}{\sigma}\int_0^s D_3(\zeta)d\zeta, \tag{75}$$

$$\rho(s) = \rho_0\exp\left(\int_0^s G(\zeta)d\zeta\right), \tag{76}$$

$$\tau(s,t) = Kt + Kp\left(\frac{2K\alpha}{\sigma} + 3p\right)\int_0^s D_3(\zeta)d\zeta + t_0, \tag{77}$$

$$\varphi(s,t) = pt + p^2\left(\frac{K\alpha}{\sigma} + 2p\right)\int_0^s D_3(\zeta)d\zeta + \phi_0, \tag{78}$$

together with the constraint conditions on the inhomogeneous fiber parameters

$$D_2(s) = \left(3p + \frac{K\alpha}{\sigma}\right)D_3(s), \tag{79}$$

$$R_1(s) = \frac{K^2(p\nu + K\gamma)}{\sigma\rho_0^2}D_3(s)\exp\left(-2\int_0^s G(\zeta)d\zeta\right), \tag{80}$$

$$R_2(s) = \frac{K^2\nu}{\sigma\rho_0^2}D_3(s)\exp\left(-2\int_0^s G(\zeta)d\zeta\right), \tag{81}$$

where the parameters K and p are related to the pulse width and phase shift, respectively, and the subscript 0 denotes the initial value of the corresponding parameters at distance $s = 0$. Thus, the general form of self-similar solutions of the generalized NLSE (64) can be obtained as

$$\Phi(s,t) = \rho_0\psi\left(\frac{K^3}{\sigma}\int_0^s D_3(\zeta)d\zeta, \tau(s,t)\right) \times \exp\left(\int_0^s G(\zeta)d\zeta + i\varphi(s,t)\right), \tag{82}$$

where $\psi(z,\tau)$ satisfies the extended NLSE with constant coefficients (1), while the functions $\tau(s,t)$ and $\phi(s,t)$ are given by Eq. (77) and (78).

Having obtained this result, we are able to construct exact self-similar solutions to Eq. (64) by using the closed-form solutions of Eq. (1) via the transformation (82). Therefore, it is significant to use the exact solutions of the constant-coefficient NLSE (1) presented above. The necessary and sufficient conditions for the existence of these self-similar solutions are given by the parametric conditions (79)–(81). The relations (75)–(78) clearly show that the third-order dispersion parameter $D_3(s)$ affects the form of the effective propagation distance, similarity variable, and phase of the self-similar pulse.

Now let us construct the exact self-similar solutions of the generalized NLSE with varying coefficients (64) by using the obtained exact solutions of the constant-coefficient NLSE (1) and the transformation (82). First we construct the families of self-similar cnoidal wave solutions of the generalized NLSE model (64). Employing the periodic bounded solutions (21) of Eq. (1) and the transformation (82) with Eqs. (75)–(78) and considering the constraint conditions (79)–(81), we have a self-similar cnoidal wave solution of Eq. (64) as

$$\Phi(s,t) = \rho_0\Lambda\exp\left(\int_0^s G(\zeta)d\zeta\right)[1 - \lambda + 2\lambda\,\mathrm{cn}^2(w\xi,k)]^{1/2}\exp[i\theta(s,t)], \tag{83}$$

where the traveling coordinate ξ is given by

$$\xi(s,t) = Kt - \eta + \left[Kp\left(\frac{2K\alpha}{\sigma} + 3p\right) - \frac{qK^3}{\sigma}\right] \times \int_0^s D_3(\zeta)d\zeta + t_0 \tag{84}$$

and the phase of field has the form

$$\theta(s,t) = \kappa z - \delta\tau + \phi + \varphi(s,t), \tag{85}$$

where z and τ are given by Eqs. (75) and (77), respectively, the phase $\varphi(s,t)$ is given by Eq. (78), and Λ and w satisfy Eq. (22).

We may also obtain a second family of exact self-similar cnoidal sn wave solutions of Eq. (64) by inserting the

solution (29) into the transformation (82) as

$$\Phi(s,t) = \rho_0 \Lambda \exp\left(\int_0^s G(\zeta)d\zeta\right) \mathrm{sn}(w\xi, k) \exp\left[i\theta(s,t)\right], \tag{86}$$

where ξ is given by Eq. (84), the phase $\theta(s,t)$ is the same expression in (85), and Λ and w satisfy Eq. (30).

A third family of exact self-similar cnoidal cn wave solutions of Eq. (64) can be obtained by substituting Eq. (34) into the transformation (82) as

$$\Phi(s,t) = \rho_0 \Lambda \exp\left(\int_0^s G(\zeta)d\zeta\right) \mathrm{cn}(w\xi, k_0) \exp\left[i\theta(s,t)\right], \tag{87}$$

where the variable ξ is given by

$$\xi(s,t) = Kt - \eta + \left[Kp\left(\frac{2K\alpha}{\sigma} + 3p\right) - \frac{q_0 K^3}{\sigma}\right] \times \int_0^s D_3(\zeta)d\zeta + t_0 \tag{88}$$

and $\theta(s,t)$ satisfies Eq. (85). Also, q_0 is shown in Eq. (9), $k_0 = 1/\sqrt{2}$, and Λ and w are given in Eq. (35).

In addition, we obtained a fourth family of exact self-similar cnoidal wave solutions of Eq. (64) by inserting the solution (38) into the transformation (82) as

$$\Phi(s,t) = \rho_0 \Lambda \exp\left(\int_0^s G(\zeta)d\zeta\right) \frac{\mathrm{sn}(w\xi, k)}{1 + \mathrm{cn}(w\xi, k)} \times \exp\left[i\theta(s,t)\right], \tag{89}$$

where ξ is given by Eq. (84), the phase $\theta(s,t)$ is the same expression in (85), and Λ and w satisfy Eq. (39).

Next we construct the exact self-similar soliton solutions of the generalized NLSE with distributed coefficients (64). Substituting the solution (23) into the transformation (82) leads to an exact self-similar bright-soliton solution of Eq. (64) of the form

$$\Phi(s,t) = \rho_0 A \exp\left(\int_0^s G(\zeta)d\zeta\right) \mathrm{sech}(w_0\xi) \exp\left[i\theta(s,t)\right], \tag{90}$$

where A and w_0 are given by Eq. (24) and ξ and $\theta(s,t)$ are given by Eqs. (84) and (85), respectively. Moreover, substitution of the solution (31) into the transformation (82) yields an exact self-similar dark-soliton solution of Eq. (64) of the form

$$\Phi(s,t) = \rho_0 B \exp\left(\int_0^s G(\zeta)d\zeta\right) \tanh(w_0\xi) \exp\left[i\theta(s,t)\right], \tag{91}$$

where B and w_0 are given by Eq. (32) and ξ and $\theta(s,t)$ are the same expressions in (84) and (85), respectively.

For the completeness of the investigation, let us discuss the propagation dynamics of the obtained self-similar structures in a specified soliton control system. We should note that for the self-similar solutions of Eq. (64), only two of the five distributed parameters $D_2(s)$, $D_3(s)$, $R_1(s)$, $R_2(s)$, and $G(s)$ in the generalized NLSE (64) are free parameters. For instance, if $D_3(s)$ and $G(s)$ are selected to be the free parameters, then the parameters $D_2(s)$, $R_1(s)$, and $R_2(s)$ will be determined from Eqs. (79), (80), and (81), respectively. To illustrate our results, we consider a soliton control system similar to the system in [44] with the periodic varying third-order dispersion and a constant gain or loss parameter [46,47]

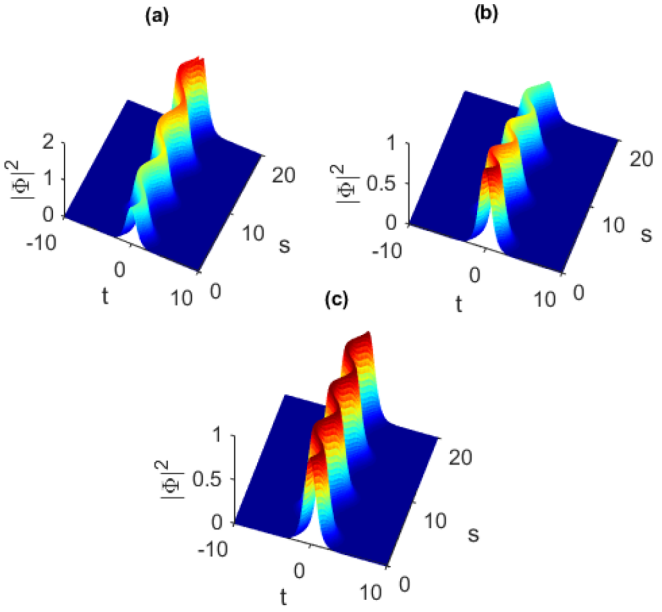

FIG. 1. Propagation dynamics of the self-similar bright soliton (90) with $D_3(s) = D_{30}\cos(gs)$ and $G(s) = G_0$ for (a) $G_0 = 0.02$, (b) $G_0 = 0.02$, and (c) $G_0 = 0$. The parameters for the bright-soliton solution with the dimensionless function $|\Phi(s,t)|^2$ and variables s and t are defined in Sec. VI.

$$D_3(s) = D_{30}\cos(gs), \quad G(s) = G_0, \tag{92}$$

where D_{30} and g are the parameters describing the third-order dispersion and G_0 denotes the constant net gain (greater than zero) or loss (less than zero). We note that the other parameters can be obtained exactly through the constraint conditions (79)–(81). For these parameter choices, the effective propagation distance given by Eq. (75) ends up being $z(s) = \frac{D_{30}K^3}{\sigma g}\sin(gs)$, indicating that z varies periodically with the original propagation distance s. Moreover, the amplitude of self-similar pulses can be determined from Eq. (76) as $\rho(s) = \rho_0 \exp(G_0 s)$. This result shows that the gain or loss coefficient affects the evolution of the self-similar pulse amplitude.

In order to demonstrate the controllable self-similar waves, here we take the self-similar bright and dark solitons (90) and (91) as an example to discuss the evolution of the obtained self-similar structures. Figure 1 depicts the propagation dynamics of the self-similar bright-soliton solution (90) with $D_3(s)$ and $G(s)$ given by Eq. (92) for the parameter values $\alpha = -2$, $\gamma = 1$, $\sigma = -0.5$, $\nu = 0.5$, and $D_{30} = -1/9$. The results for the self-similar dark-soliton solution (91) are illustrated in Fig. 2 for the values $\alpha = 0.25$, $\gamma = 1.25$, $\sigma = 0.5$, $\nu = 0.5$, and $D_{30} = 0.1875$. The other parameters are chosen as $g = 1$, $p = 1/3$, $\eta = 0$, $q = 3$, $\rho_0 = 1/\sqrt{2}$, $K = 1$, and $t_0 = 0$. From the evolution plots, we see that the self-similar structures exhibit a snakelike propagation behavior. For such an oscillatory trajectory, the self-similar optical pulse keeps its shape while propagating along the optical fiber, although its position oscillates periodically. One can also see that the self-similar soliton

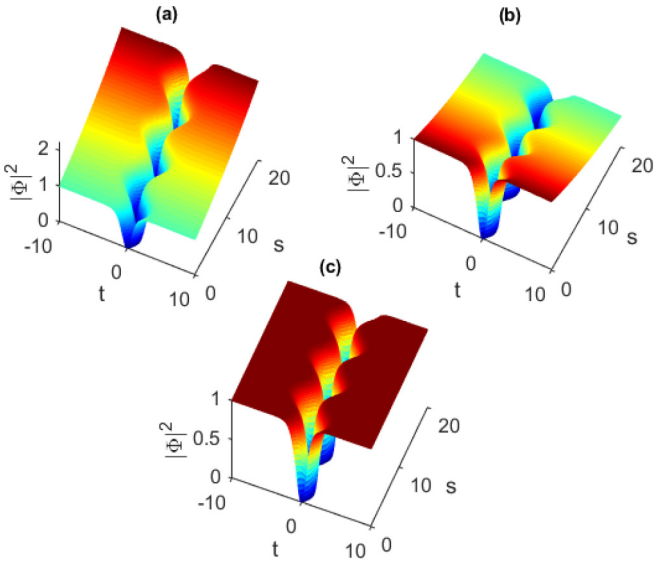

FIG. 2. Propagation dynamics of the self-similar dark soliton (91) with $D_3(s) = D_{30}\cos(gs)$ and $G(s) = G_0$ for (a) $G_0 = 0.02$, (b) $G_0 = 0.02$, and (c) $G_0 = 0$. The parameters for the dark-soliton solution with the dimensionless function $|\Phi(s,t)|^2$ and variables s and t are defined in Sec. VI.

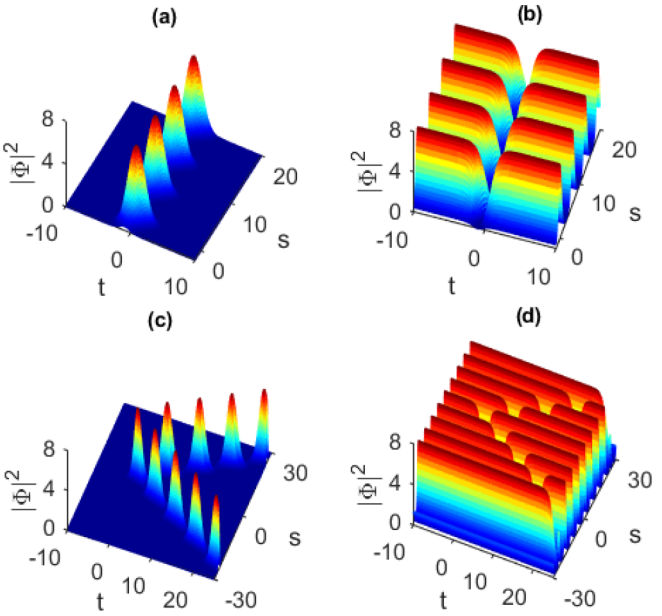

FIG. 3. Propagation dynamics of (a) the self-similar bright soliton (90) and (b) the self-similar dark soliton (91) with $D_3(s) = D_{30}\cos(gs)$ and $G(s) = \sin(z)$ and of (c) the self-similar bright soliton (90) and (d) the self-similar dark soliton (91) with $D_3(s) = D_{30}\tanh(s)$ and $G(s) = \sin(s)$. The other parameters for the bright- and dark-soliton solutions with the dimensionless function $|\Phi(s,t)|^2$ and variables s and t are the same as in Figs. 1 and 2, respectively.

amplitude increases [Fig. 1(a)] or decreases [Fig. 1(b)] along the propagation direction of the optical medium depending on the sign of G_0. For the special case of vanishing gain or loss ($G_0 = 0$), the self-similar pulse propagates in the inhomogeneous optical fiber without changing its amplitude and width [Fig. 1(c)]. It is obvious that the feature of the self-similar dark-soliton solution is the same as the bright-soliton one [Figs. 2(a)–2(c)].

Behavior completely different from the preceding self-similar pulses appears when the gain or loss function is chosen to vary periodically with the distance s as [48] $G(s) = \sin(s)$. The propagation of both self-similar bright and dark solitons in gain and loss media is shown in Figs. 3(a) and 3(b) with the same selection of the parameter $D_3(s)$ and the same parameter values as in Figs. 1 and 2, respectively. For this choice of gain or loss management, the snakelike propagation behavior disappears and we get a periodic emergence of pulses due to the presence of periodic gain [Figs. 3(a) and 3(b)].

Additionally, we have investigated the behavior of self-similar pulses in an inhomogeneous optical fiber system with varying third-order dispersion and gain or loss parameters [48]: $D_3(s) = D_{30}\tanh(s)$ and $G(s) = \sin(s)$. Figures 3(c) and 3(d) display the propagation dynamics of the self-similar bright- and dark-soliton solutions (90) and (91) for the same values of parameters as those in Figs. 1 and 2, respectively. From these figures we see that this choice of dispersion and gain or loss management leads to an interesting periodic occurrence of self-similar bright and dark solitons, as shown in Figs. 3(c) and 3(d), respectively.

Now we discuss the evolution of self-similar pulses in an exponential dispersion decreasing fiber system [44,49] with

$$D_3(s) = D_{30}\exp(-rs), \quad G(s) = G_0, \tag{93}$$

where D_{30} and r are the parameters to describe the third-order dispersion and G_0 denotes the constant net gain or loss. Then it follows from Eq. (75) that the effective propagation distance can be written as $z(s) = \frac{D_{30}K^3}{\sigma r}[1 - \exp(-rs)]$. Figure 4 displays the evolutional dynamics of the self-similar bright- and dark-soliton solutions (90) and (91) with $D_3(s)$ given by Eq. (93) and without gain ($G_0 = 0$) for the parameter $r = 0.3$. The other parameters are the same as those in Figs. 1 and 2, respectively. From this figure we can see that the self-similar pulses keep their shapes, except for the change of soliton velocity at the beginning of propagation.

Importantly, we can choose different profiles of third-order dispersion and gain (loss) parameters to control the evolution of self-similar pulses through the optical fiber system, which results in widely different shapes. The specific form of these parameters can be selected depending upon the soliton control system under study.

VII. DISCUSSION

Before concluding, let us discuss the experimental verification of the results presented here. With the current utilization of optical fibers as the transmission medium in long-distance communications systems, it becomes crucially important to know the characteristics of nonlinear operating modes in such systems. We have found that the balance among GVD, Kerr nonlinearity, third-order dispersion, and the self-steepening effect in the fiber medium described by the extended NLSE (1) gives rise to the formation of a rich variety of periodic and solitary waves. We also observed from the relations (8) and (9) that the frequency shift δ and wave number κ of such

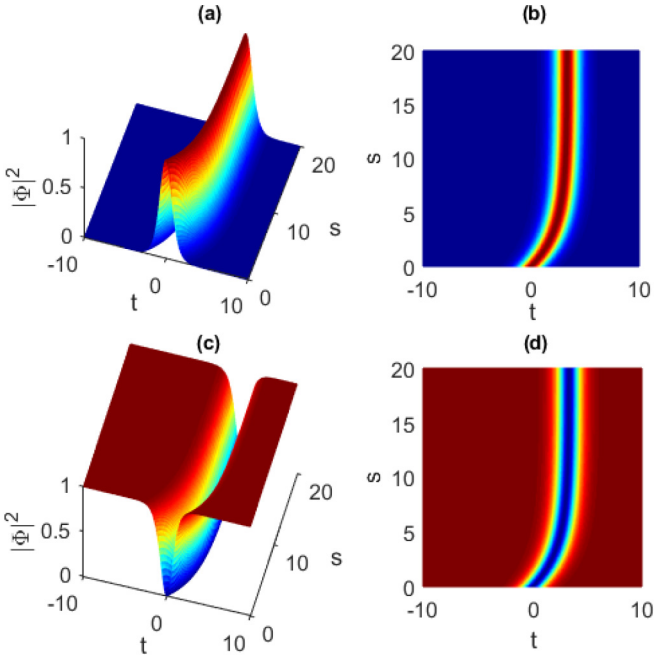

FIG. 4. Propagation dynamics of (a) and (b) the self-similar bright soliton (90) and (c) and (d) the self-similar dark soliton (91) with $D_3(s) = D_{30}\exp(-rs)$ and $G(s) = 0$. The other parameters for the dimensionless function $|\Phi(s,t)|^2$ and variables s and t are defined as in Figs. 1 and 2, respectively.

structures are strongly dependent on the fiber parameters. It is within the framework of such relationships that the fiber system allows periodic-wave and soliton-type pulse propagation. Importantly, the achievement of such necessary and sufficient conditions needs the utilization of special optical fibers.

In order to discuss the experimental possibilities to realize the obtained structures in an optical fiber, here we take the localized pulses as an example to analyze the formation of the bright soliton (23) and dark soliton (31) in the fiber system. Regarding the bright pulse (23), we have seen that the condition $\nu\sigma < 0$ is necessary for the existence of such a soliton envelope. For a conventional single-mode fiber, $\beta_3 > 0$ holds [50] (i.e., $\sigma > 0$). Moreover, the nonlinearity parameter γ takes values in the range 1–100 $\mathrm{W}^{-1}/\mathrm{km}$ if we use $n_2 = 2.6 \times 10^{-20}$ m^2/W [15]. Since $\nu = \gamma/\omega_0$, with ω_0 the signal carrier frequency, we obtain a positive value of the self-steepening parameter (i.e., $\nu > 0$) and consequently we have $\nu\sigma > 0$. As a result, the case $\beta_3 > 0$ does not allow the existence of the obtained bright-soliton pulses in conventional single-mode fibers. However, if considering the negative third-order dispersion regime, i.e., $\beta_3 < 0$, the existence condition $\nu\sigma < 0$ is readily satisfied and the fiber can support optical bright solitons. Hence, we may conclude that the condition $\beta_3 < 0$ is required for the existence of bright pulses in the present fiber system. Importantly, one can have negative values of the parameter β_3 only in overcompensated light guides with a flat dispersion curve [50].

Unlike the bright-type soliton, the dark pulse (31) existed when $\nu\sigma > 0$. For experimental verification of this kind of soliton, we may use, for example, a conventional fiber with [51] $\beta_2 = -20$ $\mathrm{ps}^2/\mathrm{km}$, $\beta_3 = 0.108$ $\mathrm{ps}^3/\mathrm{km}$, $A_{\mathrm{eff}} =$ 55 $\mu\mathrm{m}^2$, and $n_2 = 2.6 \times 10^{-20}$ m^2/W. Here A_{eff} is the effective fiber core area which is related to the core radius w of the fiber by $A_{\mathrm{eff}} = \pi w^2$ and n_2 is the nonlinear refractive index coefficient. In general, the nonlinearity coefficient is found from $\gamma = 2\pi n_2/\lambda A_{\mathrm{eff}}$ to be equal to $\gamma = 1.91$ $\mathrm{W}^{-1}/\mathrm{km}$ at the telecommunication wavelength $\lambda = 1.55$ μm. For the ultrashort laser pulse propagation through an optical fiber at the wavelength 1.55 μm and carrier frequency $\omega_0 = 1.22 \times 10^{15}$ s^{-1}, i.e., $T_0 = 5.1475 \times 10^{-15}$ s [52], we can estimate the size of the self-steepening coefficient $\nu = \gamma/\omega_0 = 0.0983$ $\mathrm{W}^{-1}/2\pi$ km THz. With this choice of fiber parameters, the condition $\nu\sigma > 0$ is readily satisfied and therefore the dark-pulse propagation can be realized experimentally. Thus we can conclude that the obtained dark solitons can be experimentally verified in conventional single-mode fibers with positive third-order dispersion (i.e., $\beta_3 > 0$). With regard to realizing such soliton pulses experimentally, several practical techniques were introduced. For example, in one method for generating dark solitons, a Mach-Zehnder modulator, driven by nearly rectangular electrical pulses, modulates the continuous-wave output of a semiconductor laser [53]. Optical switching using a fiber-loop mirror, in which a phase modulator is placed asymmetrically, can also be employed to generate solitons [54].

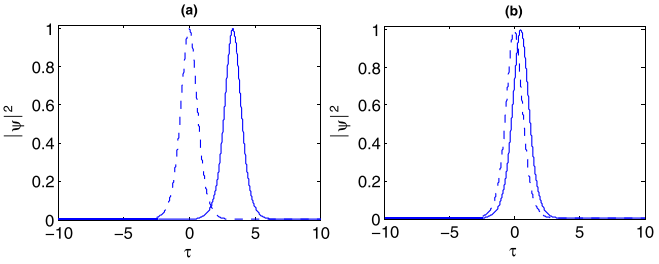

FIG. 5. Intensity profiles of the bright soliton in an optical fiber at $z = 200$ with $\gamma = 1$, $\beta_2 = -1$, and $\nu = 0.6$ for (a) $\beta_3 = -2$ and (b) $\beta_3 = -0.3$. The dashed and solid lines represent the input and output soliton pulses, respectively.

The preceding analysis has shown that the third-order dispersion and self-steepening nonlinearity play a significant role in the formation of localized pulses. We note that these higher-order effects not only play a role in the existence conditions, but also influence the characteristics of propagating solitary waves. Let us discuss numerically the impact of the third-order dispersion on soliton dynamics. Here we take the bright soliton (23) as an example to study the effect of higher order on the soliton propagation in the fiber system. To this end, we numerically integrated Eq. (1) using the exact soliton solution (23) as an initial condition. For our numerical simulation, we use the split-step Fourier method and the results are presented in Fig. 5, which shows the intensity profiles of the bright soliton under the influence of third-order dispersion when $\nu = 0.6$. Figures 5(a) and 5(b) show the input and output intensity profiles of the soliton envelope for $\beta_3 = -2$ and $\beta_3 = -0.3$, respectively. In the setting of optical fibers, it has been demonstrated that as the propagation distance increases, the positive self-steepening effect shifts the center of the generated optical pulse towards the trailing edge [15]. We can clearly see from Fig. 5(a) that the soliton is shifted towards

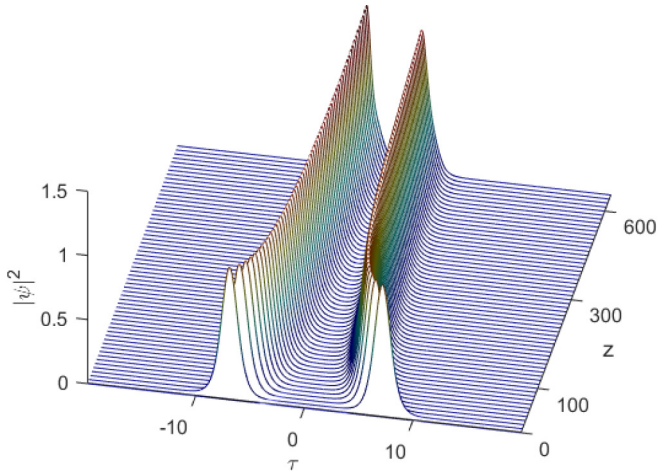

FIG. 6. Interaction scenario of two neighboring bright solitons (23) when the initial separation is equal to 7. The adopted parameters are $\gamma = 0.5$, $\beta_2 = -1.01$, $\nu = 0.01$, and $\beta_3 = -0.3$. These parameters also satisfy the stability condition in Eq. (55).

the trailing edge of the pulse. We also see that an increased value of the third-order dispersion parameter tries to bring the peak of the soliton pulse towards zero temporal shift as shown in Fig. 5(b). From this result, we can conclude that an appropriate choice of positive ν and negative β_3 can suppress the soliton shift in the optical fiber. Hence, the interplay between third-order dispersion and the self-steepening effect provides stable propagation of the soliton.

In what follows, for the completeness of the investigation, we study the soliton interaction numerically in the presence of third-order dispersion and the self-steepening effect. It of interest to know how the soliton solution (23) mutually interacts in the fiber medium under the influence of these higher-order effects. Here we can use a superposition of two soliton solution (23) profiles so that the initial pulse waveform is

$$\psi(z=0,\tau) = \psi_1(\tau) + \psi_2(\tau), \tag{94a}$$

$$\psi_1(\tau) = A_1 \mathrm{sech}[w_1(\tau + \tau_0/2)]e^{-i\delta_1\tau}, \tag{94b}$$

$$\psi_2(\tau) = A_2 \mathrm{sech}[w_2(\tau - \tau_0/2)]e^{-i\delta_2\tau}, \tag{94c}$$

where $A_{1,2}$ and $w_{1,2}$ are defined in the relation (24), $\kappa_{1,2}$ is given by (9), and τ_0 is the initial separation between the two solitons. Then we numerically simulate the interaction scenario between two neighboring soliton pulses with the initial separation $\tau_0 = 7$. Corresponding to the input waveform given by (94), we consider here the case of in-phase solitons with equal amplitudes [55]. The evolution of the soliton pair in the optical fiber is presented in Fig. 6. It can be seen from this figure that the two soliton pulses hardly interact and the separation remains constant while propagating 600 dispersion lengths along the fiber. This indicates that the interaction force between neighboring solitons is weaker in the presence of higher-order effects. However, when the initial separation decreases further, the interaction between two neighboring solitons becomes serious and repulsion occurs. Through numerical studies it was shown that third-order dispersion may suppress the collision between two in-phase pulses [56]. Here, in addition to the third-order dispersion, the self-steepening effect is taken into account and a similar result is found. It is relevant to mention that significant results have also shown that under the influence of the third-order dispersion, self-steepening, and self-frequency shift effects, the interaction between neighboring solitons can be restrained to some extent [57]. We would like to note that in our case of study, the presence of the third-order dispersion and self-steepening nonlinearity in the fiber can lead to the suppression of the two-soliton interaction, thus stabilizing the propagation of the pulse pair. This interaction process confirms the remarkable robustness of these solitons and their ability to execute stable propagation in the fiber system under the influence of higher-order effects. This property is a real advantage for experimental demonstration prospects and possible applications.

VIII. CONCLUSION

We have studied the possibility of the formation of periodic waves and localized pulses in an optical fiber medium characterized by a Kerr-type nonlinear response and exhibiting third-order dispersion and self-steepening effects. Pulse evolution in such a system is described by the extended NLSE with second- and third-order dispersions, Kerr nonlinearity, and self-steepening terms. The experimental observation of femtosecond optical solitons is possible, for example, in a silicon-on-insulator waveguide with quasi-TM polarized pulses excited along the special direction on the surface of the waveguide. The discussion that the Raman effect is absent for specially designed slot waveguides was presented in Secs. I and II, as well as appropriate references.

The regular method that we have developed for studying the existence of propagating pulses has shown that both bright and dark envelope solitons are possible within this model in the presence of all equation parameters. It was found that the soliton characteristics obtained depend on all the material parameters. The developed approach also leads to a variety of exact cnoidal wave solutions of the extended NLSE (1) expressed in term of elliptic functions like cn and sn. These cnoidal waves representing exact solutions in the form of periodic arrays of pulses to NLSE models play an important role in the analysis of the data transmission in fiber-optic telecommunications links [45]. Furthermore, we have studied analytically the stability of soliton solutions based on the theory of optical nonlinear dispersive waves [31]. The results indicate that the stability properties of these solitons depend strongly on the higher-order effects such as third-order dispersion and self-steepening nonlinearity. The modulation instability of the continuous wave propagating through the optical fiber system was also studied. It was found that the additional self-steepening term provides extra freedom to control the amplitude of the modulation instability gain profile, but the third-order dispersion does not contribute to the gain spectrum. We also examined the self-similar propagation of femtosecond light pulses inside the optical fibers within the framework of the generalized NLSE with varying dispersion, cubic nonlinearity, self-steepening, and gain or loss. By means of the similarity transformation method, we constructed the relation between this generalized wave equation and the related constant-coefficient one. Then, based on the resulting transformation, we presented exact self-similar

cnoidal wave solutions as well as self-similar bright- and dark-soliton solutions under certain parametric conditions. We further discussed the dynamical behavior of self-similar structures in the dispersion changing periodically fiber system and an exponentially varying dispersion medium. We observed that the soliton shape can be controlled by selecting the third-order dispersion and the gain or loss parameters appropriately.

Characteristics and stability properties of the localized structures and theoretical modeling of the underlying NLSE with the third-order dispersion and self-steepening nonlinearity indicate the potential relevance of the obtained envelope solitons for the experiments on the short-pulse propagation in optical fiber communications, ultrafast lasers, and slow-light devices.

[1] L. F. Mollenauer, R. H. Stolen, and J. P. Gordon, Phys. Rev. Lett. **45**, 1095 (1980).

[2] F. Salin, P. Grangier, G. Roger, and A. Brun, Phys. Rev. Lett. **56**, 1132 (1986).

[3] J. S. Aitchison, A. M. Weiner, Y. Silberberg, M. K. Oliver, J. L. Jackel, D. E. Leaird, E. M. Vogel, and P. W. E. Smith, Opt. Lett. **15**, 471 (1990).

[4] G. P. Agrawal, *Applications of Nonlinear Fiber Optics* (Academic, San Diego, 2001).

[5] P. Di Trapani, D. Caironi, G. Valiulis, A. Dubietis, R. Danielius, and A. Piskarskas, Phys. Rev. Lett. **81**, 570 (1998).

[6] V. E. Zakharov and A. B. Shabat, JETP **61**, 118 (1972) [Sov. Phys. JETP **34**, 62 (1972)]; **64**, 1627 (1973) [**37**, 823 (1973)].

[7] S. A. Ponomarenko, N. M. Litchinitser, and G. P. Agrawal, Phys. Rev. E **70**, 015603(R) (2004).

[8] C. E. Zaspel, Phys. Rev. Lett. **82**, 723 (1999).

[9] U. Peschel, C. Etrich, F. Lederer, and B. A. Malomed, Phys. Rev. E **55**, 7704 (1997).

[10] Y. Song, X. Shi, C. Wu, D. Tang, and H. Zhang, Appl. Phys. Rev. **6**, 021313 (2019).

[11] Y. Song, Z. Wang, C. Wang, K. Panajotov, and H. Zhang, Adv. Photon. **2**, 024001 (2020).

[12] Y. Song, S. Chen, Q. Zhang, L. Li, L. Zhao, H. Zhang, and D. Tang, Opt. Express **24**, 25933 (2016).

[13] A. Mohamadou, B. E. Ayissi, and T. C. Kofané, Phys. Rev. E **74**, 046604 (2006).

[14] Alka, A. Goyal, R. Gupta, C. N. Kumar, and T. S. Raju, Phys. Rev. A **84**, 063830 (2011).

[15] G. P. Agrawal, *Nonlinear Fiber Optics*, 5th ed. (Academic, New York, 2013).

[16] *Optical Solitons Theory and Experiment*, edited by J. R. Taylor (Cambridge University Press, New York, 1992).

[17] V. M. Lashkin, Phys. Rev. E **69**, 016611 (2004).

[18] K. Porsezian and K. Nakkeeran, Phys. Rev. Lett. **76**, 3955 (1996).

[19] N. N. Akhmediev and A. Ankiewicz, *Solitons: Nonlinear Pulses and Beams* (Chapman and Hall, London, 1997).

[20] S.-H. Han and Q.-H. Park, Phys. Rev. E **83**, 066601 (2011).

[21] K. Porsezian and K. Nakkeeran, Phys. Rev. Lett. **74**, 2941 (1995).

[22] Y. Kodama, J. Stat. Phys. **39**, 597 (1985); Y. Kodama and A. Hasegawa, IEEE J. Quantum Electron. **23**, 510 (1987).

[23] N. Sasa and J. Satsuma, J. Phys. Soc. Jpn. **60**, 409 (1991).

[24] M. Gedalin, T. C. Scott, and Y. B. Band, Phys. Rev. Lett. **78**, 448 (1997).

[25] D. Mihalache, N. Truta, and L. C. Crasovan, Phys. Rev. E **56**, 1064 (1997).

[26] N. Akhmediev and M. Karlsson, Phys. Rev. A **51**, 2602 (1995).

[27] D. Artigas, L. Torner, J. P. Torres, and N. N Akhmediev, Opt. Commun. **143**, 322 (1992).

[28] Z. H. Li, L. Li, H. P. Tian, and G. S. Zhou, Phys. Rev. Lett. **84**, 4096 (2000).

[29] A. Choudhuri and K. Porsezian, Opt. Commun. **285**, 364 (2012).

[30] V. I. Kruglov and H. Triki, Phys. Rev. A **102**, 043509 (2020).

[31] H. Triki and V. I. Kruglov, Phys. Rev. E **101**, 042220 (2020).

[32] Y. S. Kivshar and G. P. Agrawal, *Optical Solitons From Fibers to Photonic Crystals* (Academic, New York, 2003).

[33] Q. Lin, O. J. Painter, and G. P. Agraval, Opt. Express **15**, 16604 (2007).

[34] Q. Lin, J. Zhang, P. M. Fauchet, and G. P. Agrawal, Opt. Express **14**, 4786 (2006).

[35] N. Tzoar and M. Jain, Phys. Rev. A **23**, 1266 (1981).

[36] D. Anderson and M. Lisak, Phys. Rev. A **27**, 1393 (1983).

[37] S.-l. Liu and W.-z. Wang, Phys. Rev. E **49**, 5726 (1994).

[38] G. B. Whitham, J. Fluid Mech. **27**, 399 (1967).

[39] A. Choudhuri and K. Porsezian, Phys. Rev. A **85**, 033820 (2012).

[40] G. P. Agrawal, Phys. Rev. Lett. **59**, 880 (1987).

[41] F. Abdullaev, S. Darmanyan, and P. Khabibullaev, *Optical Solitons* (Springer, Berlin, 1991).

[42] L. Wang, J.-H. Zhang, C. Liu, M. Li, and F.-H. Qi, Phys. Rev. E **93**, 062217 (2016).

[43] C.-Q. Dai, J.-F. Ye, and X.-F. Chen, Opt. Commun. **285**, 3988 (2012).

[44] C.-Q. Dai, G.-Q. Zhou, and J.-F. Zhang, Phys. Rev. E **85**, 016603 (2012).

[45] C. Dai, Y. Wang, and C. Yan, Opt. Commun. **283**, 1489 (2010).

[46] J. Zhang, Q. Yang, and C. Dai, Opt. Commun. **248**, 257 (2005).

[47] R. Yang, L. Li, R. Hao, Z. Li, and G. Zhou, Phys. Rev. E **71**, 036616 (2005).

[48] J.-F. Zhang, C.-Q. Dai, Q. Yang, and J.-M. Zhu, Opt. Commun. **252**, 408 (2005).

[49] R. Hao, L. Li, Z. Li, and G. Zhou, Phys. Rev. E **70**, 066603 (2004).

[50] A. B. Grudinin, V. N. Men'shov, and T. N. Fursa, JETP **70**, 249 (1990).

[51] A. Govindaraji, A. Mahalingam, and A. Uthayakumar, Optik **125**, 4135 (2014).
[52] A. Choudhuri and K. Porsezian, Phys. Rev. A **88**, 033808 (2013).
[53] W. Zhao and E. Bourkoff, Opt. Lett. **15**, 405 (1990); J. Opt. Soc. Am. B **9**, 1134 (1992).
[54] O. G. Okhotnikov and F. M. Araujo, Electron. Lett. **31**, 2197 (1995).
[55] A. Biswas, J. Nonlinear Opt. Phys. Mater. **08**, 483 (1999).
[56] P. L. Chu and C. Desem, Electron. Lett. **21**, 228 (1985).
[57] Z. Xu, L. Li, Z. Li, and G. Zhou, Opt. Commun. **210**, 375 (2002).